Impedance spectroscopy characterization of neutron irradiated thermoelectric modules for space nuclear power

Cite as: AIP Advances **9**, 055006 (2019); https://doi.org/10.1063/1.5095619
Submitted: 11 March 2019 . Accepted: 26 April 2019 . Published Online: 08 May 2019

Ramy Mesalam, Hugo R. Williams, Richard M. Ambrosi, Daniel P. Kramer, Chadwick D. Barklay, Jorge García-Cañadas, Keith Stephenson, and David P. Weston

Impedance spectroscopy characterization of neutron irradiated thermoelectric modules for space nuclear power

Cite as: AIP Advances 9, 055006 (2019); doi: 10.1063/1.5095619
Submitted: 11 March 2019 • Accepted: 26 April 2019 •
Published Online: 8 May 2019

Ramy Mesalam,[1,a)] Hugo R. Williams,[1] Richard M. Ambrosi,[2] Daniel P. Kramer,[3] Chadwick D. Barklay,[3] Jorge García-Cañadas,[4] Keith Stephenson,[5] and David P. Weston[1]

AFFILIATIONS

[1]Department of Engineering University of Leicester, Leicester LE1 7RH, UK
[2]Department of Physics & Astronomy, University of Leicester, Leicester LE1 7RH, UK
[3]University of Dayton Research Institute, 300 College Park, Dayton, Ohio 45469-0102, USA
[4]Department of Industrial Systems Engineering and Design, Universitat Jaume I, 12071 Castellón, Spain
[5]European Space Agency, ESTEC TEC-EP, Keplerlaan 1, 2201AZ Noordwijk, The Netherlands

[a)]rm467@le.ac.uk

ABSTRACT

The European Space Agency is currently supporting the research and development of advanced radioisotope power systems utilising thermoelectric modules. The performance of thermoelectric modules following exposure to neutron radiation is of significant interest due to the likely application of radioisotope thermoelectric generators in deep space exploration or planetary landers requiring prolonged periods of operation. This study utilises impedance spectroscopy to characterise the effects of neutron irradiation on the performance of complete thermoelectric modules, as opposed to standalone material. For a 50 W_e americium-241 radioisotope thermoelectric generator design, it is estimated that the TE modules could be exposed to a total integrated flux of approximately 5×10^{13} neutrons cm^{-2} (>1 MeV). In this study, an equivalent neutron dose was simulated experimentally via an acute 2-hour exposure in a research pool reactor. Bi_2Te_3-based thermoelectric modules with different leg aspect ratios and microstructures were investigated. Gamma-ray spectroscopy was initially used to identify activated radionuclides and hence quantify irradiation induced transmutation doping. To evaluate the thermoelectric properties pre- and post-irradiation, impedance spectroscopy characterization was employed. Isochronal thermal annealing of defects imparted by the irradiation process, revealed that polycrystalline based modules required significantly higher temperature than those with a monolithic microstructure. Whilst this may indicate a greater susceptibility to neutron irradiation, all tested modules demonstrated sufficient radiation hardness for use within an americium-241 radioisotope thermoelectric generator. Furthermore, the work reported demonstrates that impedance spectroscopy is a highly capably diagnostic tool for characterising the in-service degradation of complete thermoelectric devices.

I. INTRODUCTION

Space nuclear power systems are presently under development as part of a European Space Agency (ESA) funded programme.[1] These systems could potentially supply electrical and thermal energy derived from the radiogenic decay of sintered radioisotope oxide pellets. Technology such as this is a key enabler for a range of mission scenarios,[2,3] providing more science return and increased mission duration. The European Radioisotope Thermoelectric Generator (RTG) development programme has selected Americium-241 as a fuel source.[4,5] Initial design studies and a successful laboratory breadboard experimental campaign have demonstrated that bismuth telluride based (Bi_2Te_3-based) thermoelectric (TE) modules are a viable power conversion option with proven

commercial manufacturing routes.[6] Nevertheless, the long-term (≥10 years) performance and stability of Bi_2Te_3-based TE modules within an Americium-241 system is still to be investigated.

During mission operation, RTG systems will be subject to bombardment by particulate and electromagnetic radiation from both external and internal sources. Since the dose from the external environment is highly mission dependent, this study only focuses on effects linked to the decay of an internal radioisotope fuel. Americium-241 mainly decays via alpha emission, accompanied by gamma-rays. However, for Americium-241 to be a chemically stable heat source, operating safely under a required envelope of high temperatures (<1000 °C), it must be utilised in oxide form. If naturally occurring air is used for sintering, oxygenated Americium-241 will act as a high energy (~5 MeV) neutron source owing to the large alpha-neutron (α, η) reaction cross-sections of heavy oxygen isotopes.[7] Using a Monte Carlo N-Particle (MCNP) model, O'Brien *et al.*[7] predicted that the use of oxygenated Americium-241 as a pure or cermet (ceramic-metallic) fuel source will generate low energy alpha and gamma emissions, as well as a significant bi product of fast (>1 MeV) neutrons. It is well known that electronic materials are highly susceptible to random defects which can occur when a highly energetic particle (such as a fast neutron) causes disruption to their electronic structure and thus correct operation.[8] Since the design of RTGs require their TE modules to be in close proximity with the nuclear heat source (Fig. 1), the consequential effect of such irradiation on their TE efficiency over a nominal RTG lifespan is of significant interest.

In most cases, TE efficiency in materials can be assessed using a dimensionless figure-of-merit, $ZT = S^2T/\rho\lambda$, consisting of absolute temperature T and three fundamental TE parameters: Seebeck coefficient S, electrical resistivity ρ and thermal conductivity λ. Impedance spectroscopy (IS) has shown considerable promise as a tool to parametrically characterise all fundamental TE properties of TE modules without the need of multiple measurement tools.[9,10] This approach focuses on the measurement of impedance (voltage-current ratio) as a function of frequency (impedance spectrum) by applying sequential single-frequency signals (voltage or current) to the system. The experimentally obtained impedance spectrum is after which fitted to theoretically derived impedance functions (equivalent circuits), allowing for material property characterization.[11] More recently, a new comprehensive impedance function was derived which integrated all relevant transport phenomena, giving accuracy and confidence suitable for practical use.[12] The work reported in this paper demonstrates the use of the impedance spectroscopy technique to diagnose in-service degradation. Since many types of degradation mechanisms can exist for practical TE modules,[13,14] being able to characterise and monitor the influence of degradation mechanisms on TE properties is highly desirable.

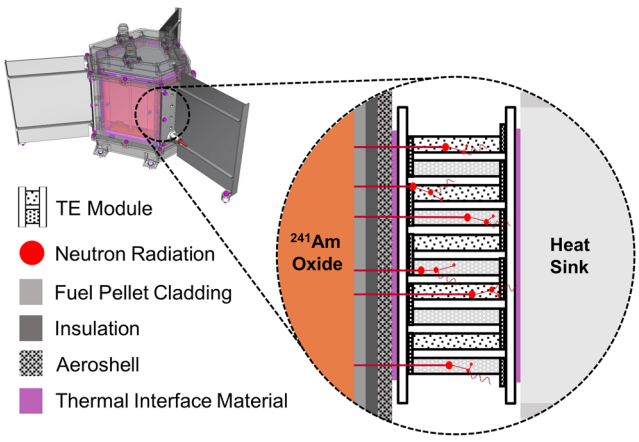

FIG. 1. European RTG concept design with TE module interface illustration.

To date, most experimentation involving neutron radiation-induced damage of TE materials, particularly Bi_2Te_3-based alloys, was carried out during the 1960s (Table I) utilising orders of magnitude higher total fluxes compared to the anticipated total flux in an Americucium-241 fueled RTG. The work covered in this era made use of multiple primitive TE measurement systems which were in their infancy.[18–20] As a result, a lack of reference materials and standardisation was present at the times.[21,22] Nevertheless, material-level studies outlined in Table I, which also includes more recent work by Wang *et al.*,[15] primarily indicate that when a typical TE material is neutron irradiated with a sufficiently long flux time and maintained at a sufficiently low temperature, the electrical resistivity consistently increased while the Seebeck coefficient either simultaneously increased or in rare cases underwent a polarity change. It is hypothesised that this occurrence is brought about by the existence of the Wigner effect. The Wigner effect describes the collision of fast neutrons with atoms within a material's crystal lattice which inevitably induces Frenkle disorder (vacancies and interstitials).[23] In turn, this contributes to the trapping of charge carriers, effectively decreasing carrier concentration and therefore resulting in the observed increase in electrical resistivity,[24] as well as in accordance with the Pisarenko relation,[25] the consequential alteration of the Seebeck coefficient. An increase in internal electrical resistance would have detrimental effects on module-level zT and desired match loading conditions, while a polarity reversal of individual thermoelements within a module would generate high resistance bridges which could render the device inoperative.

When evaluating both properties as a TE power factor (S^2/ρ), an overall decrease is exhibited due to the relatively higher increase in electrical resistivity. However, the study by Wang *et al.*[15] intriguingly identified an enhancement for n-type materials. To combat a decrease in TE power factor and therefore a proportional decrease in ZT, a reduced thermal conductivity would be required. While some studies summarised in Table I do indeed report a small reduction in measured thermal conductivity, it is ineffective at recovering a loss in ZT due to the relatively higher loss observed in TE power factor. To recover the performance of post-irradiated Bi_2Te_3-based alloys, it was shown by Corelli *et al.*[17] that an annealing temperature in the vicinity of 473 K, with a sufficiently long soak time, is required to fully reverse irradiation effects. With sufficient thermal annealing, both vacancies and interstitials become mobile, providing a mechanism by which an interstitial atom can migrate back to a vacancy and annihilate (recombination).[24] This in turn restores the previously altered carrier concentration and therefore their TE properties as reported by the authors in Table I. Understanding the sensitivity of this mechanism is fundamental in predicting the behaviour

TABLE I. Room temperature pre- (0) and post-irradiation (1) relative TE properties of bismuth telluride-based alloys for a given total neutron flux and irradiation temperature T_{rad}. Negative Seebeck coefficient ratios are indicative of a documented polarity reversal.

Authors	Year	Specimen	Total Flux (n cm^{-2}) Thermal	Total Flux (n cm^{-2}) >1 Mev	T_{rad} (K)	$\frac{S^1}{S^0}$	$\frac{\rho^1}{\rho^0}$	$\frac{\lambda^1}{\lambda^0}$	$\frac{ZT^1}{ZT^0}$
Wang *et al.*[15]	2017	Bi_2Te_3 -n type	1.3×10^{18}	1.3×10^{18}	450 – 475	1.20	1.20	1.00	1.20
Wang *et al.*[15]	2017	Bi_2Te_3 -p type	1.3×10^{18}	1.3×10^{18}	450 – 475	1.00	1.03	1.12	0.80
Idnurm *et al.*[16]	1967	Bi_2Te_3 -n type	2.0×10^{18}			1.03	1.13	0.96	0.98
Idnurm *et al.*[16]	1967	Bi_2Te_3 -p type	2.0×10^{18}			1.00	1.13	0.98	0.90
Idnurm *et al.*[16]	1967	Bi_2Te_3 - Sb_2Te_3 -n type	2.0×10^{18}			0.95	1.18	0.97	0.79
Idnurm *et al.*[16]	1967	Bi_2Te_3 - Sb_2Te_3 -p type	2.0×10^{18}			0.99	0.93	1.02	1.03
Corelli *et al.*[17]	1960	Bi_2Te_3 -n type	1.4×10^{20}	1.6×10^{19}	320 – 340	1.16	5.00	0.88	0.31
Corelli *et al.*[17]	1960	Bi_2Te_3 -n type		1.6×10^{19}	320 – 340	1.04	2.60		
Corelli *et al.*[17]	1960	Bi_2Te_3 -p type	1.4×10^{20}	1.6×10^{19}	320 – 340	−1.05	2.00		
Corelli *et al.*[17]	1960	Bi_2Te_3 -p type		1.6×10^{19}	320 – 340	−0.82	1.2		

of TE devices within an RTG environment. Furthermore, for an Americium-241 based RTG system the Aeroshell hot (~473 K) and radiator cold (~273 K) side temperatures will be such that the average operating temperature across each module will likely be closer to 373 K. Stipulating a possible susceptibility to neutron irradiation degradation.

In this work, candidate Bi_2Te_3-based modules of different aspect ratios and microstructures were irradiated with a neutron fluence of 5×10^{13} neutrons cm^{-2} (>1 MeV), equivalent to the neutron yield expected from a 50 W_e Americium-241 powered RTG containing 10 kg of oxide fuel with a nominal mission time of 10-years. By employing IS measurements in association with a previously published analytical impedance function,[14] the coherent acquisition of all TE properties for each module was assessed for pre-, post-irradiation and post-irradiation-annealed (post thermal annealed) spectra. To the authors knowledge this is the first time a single characterization technique has been used to measure service induced degradation in all fundamental TE properties for an entire TE device. Ergo, this is the first time the effects of neutron bombardment on TE modules have been characterized at a device level. The differences between modules manufactured with monolithic (directionally solidified) and polycrystalline (spark plasma sintering) TE material are also being reported. Ultimately this study demonstrates the potential application of IS characterization for assessing and monitoring the health of practical TE devices.

II. EXPERIMENTAL SET-UP AND PROCEDURE

A. Impedance spectroscopy technique

IS measurements were carried out using a Galvano-Potentiostat PGSTAT302N equipped with a FRA2 impedance module (Metrohm Autolab B. V.) at constant ambient temperature T_i (293 ± 1 K) with each TE module suspended in still air and placed within a Faraday cage to minimize external electromagnetic interference. The measurement bench was configured using 4 ultra-low impedance wires in a two-terminal configuration. Characterization was performed in galvanostatic mode in a frequency range from 1 mHz to 1 MHz (50 logarithmic increments) with an amplitude of 3 mA in the ac regime without dc bias (0 A dc). In all tests, parasitic inductance was found to be dominant for frequencies ≥4 kHz. This primarily originates from the configuration of the setup, including the cables used. This section of the spectrum has therefore been windowed in order to isolate the impedance response of the TE modules tested. Experimental observations were logged using Nova (Metrohm Autolab B. V.) and fitted to a previously derived analytical impedance function.[12] Since this study is only concerned with room temperature characterization, the previously reported function was simplified by neglecting internal-external losses via thermal radiation. The resulting function used $Z(j\omega)$ is expressed algebraically below and as an equivalent circuit in Fig. 2.

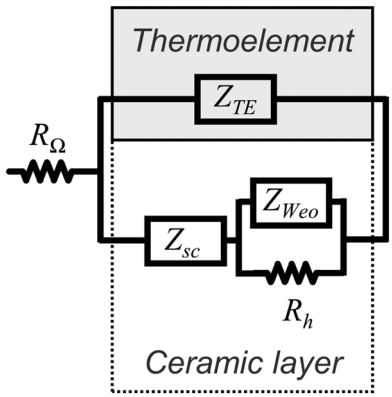

FIG. 2. Complete equivalent circuit for the corresponding impedance function. The equivalent circuit elements framed in the dotted line are related to the ceramic layers. The ones framed by the solid line in grey correspond to the thermoelectric legs (thermoelements).

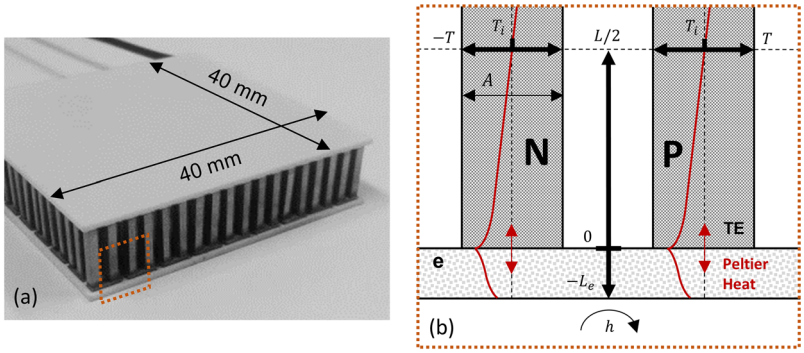

FIG. 3. (a) Thermoelectric module. (b) Axisymmetric model of an integrated thermocouple capped by an external alumina layer (e). Included is, the direction of the conductive heat fluxes induced by the Peltier heat at the junction, the absolute temperature (T), external convection (h) and geometric dimensions. A qualitive thermal profile for each thermoelement (TE) with either a negative (N) or positive (P) Seebeck coefficient under a positive current is shown in red.

$$Z(j\omega) = R_\Omega + \left(Z_{TE}^{-1} + Z_e^{-1}\right)^{-1} \tag{1}$$

$$Z_{TE} = R_{TE}\left(\frac{j\omega}{\omega_{TE}}\right)^{-0.5}\tanh\left(\frac{j\omega}{\omega_{TE}}\right)^{0.5} \tag{2a}$$

$$Z_e = Z_{sc} + \left(R_h^{-1} + Z_{Weo}^{-1}\right)^{-1} \tag{2b}$$

$$Z_{sc} = 4R_e\sum_{n=1}^{\infty}\left[\frac{J_1^2\left(\delta_n\eta^{0.5}\right)\coth\left(\eta\delta_n^2\left(\frac{\pi L_e^2}{A}\right)+\frac{j\omega}{\omega_e}\right)^{0.5}}{\delta_n^2 J_0^2(\delta_n)\left(\eta\delta_n^2\left(\frac{\pi L_e^2}{A}\right)+\frac{j\omega}{\omega_e}\right)^{0.5}}\right] \tag{2c}$$

$$Z_{Weo} = \eta R_e\left(\frac{j\omega}{\omega_e}\right)^{-0.5}\coth\left(\frac{j\omega}{\omega_e}\right)^{0.5} \tag{2d}$$

$$\omega_{TE} = \frac{4\alpha_{TE}}{L^2}, \omega_e = \frac{\alpha_e}{L_e^2} \tag{3}$$

$$R_{TE} = \frac{2NS^2T_iL}{A\lambda_{TE}}, R_e = \frac{4NS^2T_iL_e}{A\lambda_e}, R_h = \frac{R_e\lambda_e}{hL_e} \tag{4}$$

where R_Ω is the ohmic resistance of the system and R_{TE}, R_e and R_h are characteristic resistances which relate to energy losses in the system due to the TE legs, the external alumina layers, existence of a Seebeck voltage and external convection, respectively (see, Fig. 3). The former three resistances can be used to characterise all TE properties of a module,

$$\rho = \frac{R_\Omega A}{2NL}, S = \sqrt{\frac{R_eA\lambda_e}{4NT_iL_e}}, \lambda_{TE} = \frac{\lambda_eR_eL}{2R_{TE}L_e}, zT = \frac{R_{TE}}{R_\Omega} \tag{5}$$

All variable definitions can be found in the included nomenclature (see Nomenclature).

Using a complex non-linear least square fitting routine, written in a Matlab (The Mathworks, Inc., MA, USA) programming environment, resistances R_Ω, R_{TE} and R_e and angular frequencies ω_{TE} and ω_e were set as free variables to be fitted. The fitted resistances were subsequently used in Eq. 5 to calculate corresponding TE properties of the module. Additionally, R_Ω, R_{TE} and R_e can graphically be related to the axial components Z' of a Nyquist plot (Fig. 4) and therefore relative Z' changes observed in measured spectra can easily be correlated with TE property changes due to their proportionality (Eq. 5).

B. Modules tested

For this study, five commercially manufactured (Nanoforce Ltd, European Thermodynamics Ltd) Bi_2Te_3-based TE modules were procured with different leg aspect ratios, see Table II. All modules include monolithic n-type Te-doped Bi_2Te_3, Pb/Sn soldered joints and copper contacts. Regarding their p-type composition, modules 1 – 4 contain monolithic Sb-doped Bi_2Te_3, while module 5 utilises polycrystalline $Bi_{0.5}Sb_{1.5}Te_3$. Properties common to all modules are reported in Table III. Module 1 was used as an experimental control.

C. Irradiation procedure

To experimentally simulate neutron irradiation from a 200 W_{th} Americium-241 RTG fuel source, each TE module was subjected to an acute exposure in a 500 kW_{th} research pool reactor (Fig. 5) at The Ohio State University – Nuclear Reactor Lab for an equivalent

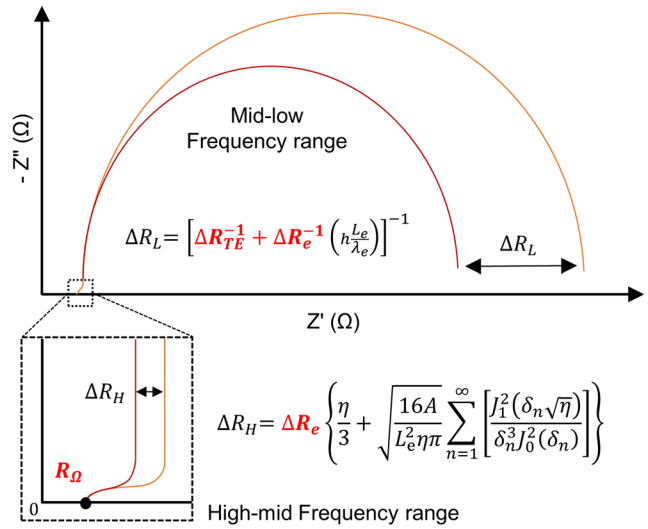

FIG. 4. Characteristic Nyquist plot of a commercial thermoelectric module and the response to varying characteristic resistances.

TABLE II. Thermoelectric module specific geometry.

	TE Leg Length, L (mm)	TE Leg Aspect Ratio
Module 1 (Control)	4	0.30
Module 2 and 3	8	0.15
Module 4 and 5	6	0.20

fluence of ~5 × 10^{13} neutrons cm^{-2}. The TE modules in question were suspended (Fig. 5a) inside a cadmium sheet wrapped NalGene container (Fig. 5b), with the TE modules alumina isolation cover plates being carefully positioned so as to face perpendicular to oncoming neutrons. The cadmium was employed to allow the absorption of thermal neutrons, to isolate the dosage to fast neutron fluxes (>1 MeV), which is more representative of neutron yields expected from an Americium-241 based RTG. Given the requirement that a single 50 W_e Americium-241 powered RTG shall have an estimated lifespan of 10-years, 5-years of initial exposure (e.g. system assembly and integration, storage, transfer to launch site, spacecraft integration, launch) plus 5-years of nominal mission exposure, an equivalent neutron fluence for each TE modules was estimated as follows.

For an Americium-241 (~0.1 W_{th} g^{-1}) powered RTG to produce 50 W_e using a Bi_2Te_3-based TE generator (conversion efficiency ~5%), 10 kg of Americium-241 oxide is required to thermally decay an equivalency of 1 kW_{th}. If the oxide fuel employs naturally occurring oxygen isotropic ratios and no oxygen exchange takes place, a gram of oxygenated Americium-241 in AmO_2 form will potentially generate around 5 × 10^3 neutrons s^{-1},[7] hence an RTG with 10 kg of oxide fuel will generate an estimated neutron flux of 5 x 10^7 neutrons s^{-1}. Assuming 10 years (3.2 × 10^8 s) nominal operational life, an RTG of this caliber would produce a total neutron yield of 1.6 × 10^{16} neutrons at its end-of-life. The distance between the TE modules and the fuel centerline is estimated as 5 cm based on the current design, which gives a projected spherical surface area of the radiative source of 314 cm^2. It can therefore be estimated that a single TE module will potentially be exposed to a neutron fluence of 5 x 10^{13} neutrons cm^{-2}. It should be noted that this calculation is likely an over estimation as it neglects shielding from encapsulation and interfacial

TABLE III. Room temperature properties shared by all tested thermoelectric modules.

Geometric Properties	
No. of TE Couples, N	161
Alumina Layer Thickness, L_e (mm)	0.8
TE Leg Cross-sectional Area, A (mm^2)	1.44
TE Module Alumina Outer Area, A_o (mm^2)	40 × 40
Filling Factor, $\eta = 2A(N+1)/A_o$	0.29
Thermophysical Properties	
Alumina Thermal Conductivity, λ_e (W m^{-1} K^{-1})[29]	30
Alumina Thermal Diffusivity, α_e (m^2 s^{-1})[14]	1.2 × 10^{-5}
Convective Heat Transfer Coefficient, h (W m^{-2} K^{-1})[14]	25

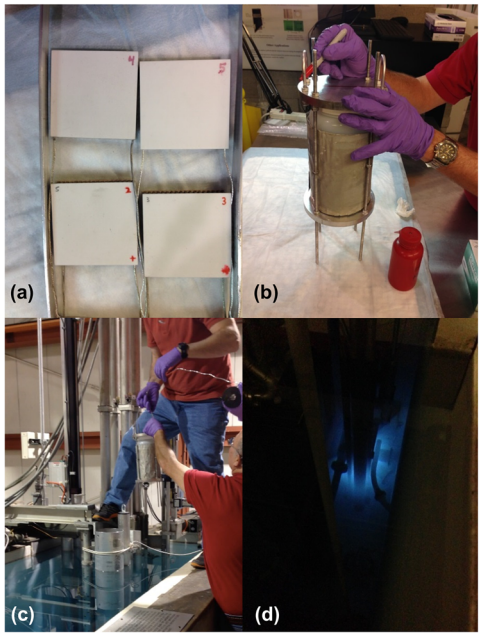

FIG. 5. (a) Pre-irradiated modules suspended from a metal hanger prior to being placed within the shielded container. (b) Container setup prior to being placed down the pool reactor dry tube. (c) Container being placed down pool reactor dry tube. (d) Cherenkov glow from the pool reactor during module irradiation.

materials illustrated in Fig. 1 and research is still ongoing to decide which chemical form of the oxide fuel (AmO_2, Am_2O_3 or mixed) should be used.[4,5] Although, since actual mission durations for RTG systems have historically shown to be repeatedly extended beyond their initial operational phase to achieve a greater science return (e.g. Voyager, Galileo, Ulysses, Cassini, New Horizons and Mars Science Laboratory missions), an over estimation in the perceived neutron fluence is justifiable.

The container enclosing the TE modules was positioned within the reactor pool via a movable dry tube (Fig. 5c) which was carefully positioned radial in relation to the reactor to approximately recreate the same neutron fluence exposure over an acute 2-hour period (Fig. 5d). while it is known a chronic (long-term) exposure would be more representative of an RTG system, the experimental time required to duplicate this is unreasonable. Throughout neutron exposure the ambient temperature inside the container was kept well below the minimum annealing temperature of 473 K, indicated by historical data.[15–17] This was achieved using a relatively low total fluence and making use of the reactor's cooling pool which maintains an average equilibrium bulk temperature of 293 ± 10 K.

Once safely extracted from the dry tube, the container was placed within a high purity germanium (HPGe) gamma-ray spectroscopy detector for spectrographic analysis. Short- and long-lived radioactive nuclei (radionuclides) were characterized and collected by a dedicated Lynx™ MCA followed by subsequent analysis using Genie™ 2000 gamma-ray analysis software. Characterization was first performed shortly after irradiation, followed by one week later

and lastly after a total decay period of two months. A measurement calibration was not performed for the container configuration and therefore the obtained branching ratios (yield %) should only be taken as magnitude accurate. Once activity reached an exempt quantity (below background), the container was shipped back to the University of Leicester where post-irradiation IS was performed on each TE module and compared to pre-irradiation data.

D. Thermal annealing procedure

Isochronal thermal annealing was performed on all post-irradiated TE modules using a convection oven to test the thermal stability of radiation-induced defects. Starting at room temperature (293 K), annealing was undertaken over increasing increments of 25 K (1-hour soak time). After each incremental anneal, a post-irradiation-annealed impedance spectrum was measured. This sequence was continuously performed until a full defect anneal was observed in the subsequent post-irradiation-annealed impedance spectrum or the maximum service temperature (423 K) of the cold side solder was reached.

III. RESULTS AND DISCUSSION

A. Gamma-ray spectroscopy

Prior to characterization, it was noted that discoloration of the external alumina substrates was found to be present for all post-irradiated modules, see Fig. 6 for an example. The discoloring of post-irradiated alumina is well documented in the open literature and is said to be caused by the generation of intrinsic point defects, namely oxygen vacancies.[26] These vacancies can be filled by one or more unpaired electrons which in turn tend to absorb light in the visible spectrum, forming color centers. While there are some reports in the open literature of cases where color centers were annealed out in the range of 400 – 1000 K,[26] in this study a maximum isochronal thermal anneal at 423 K for 1 hour was found to not be sufficient to cause a visible reduction in discoloration.

Figure 7 shows the gamma-ray spectroscopy analysis of activated nuclides one week after the irradiation procedure. Since that time, many short-lived nuclides that were initially counted, Na-24, Mn-54, Cu-64, Sb-122 and La-140 were no longer detected. The longer lasting nuclides observed can be said to originate from the transmutation of lead solder joints (Sn-117m, 158.6 KeV) as well as tellurium (Te-123m, 159.0 KeV and I-131, 364.5 KeV)

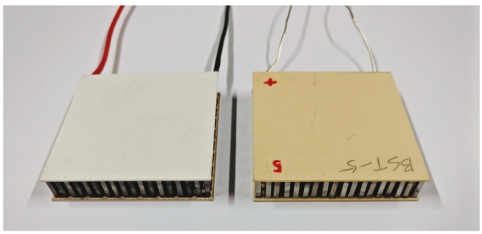

FIG. 6. A non-irradiated module (left) and post neutron irradiated module 5 (right).

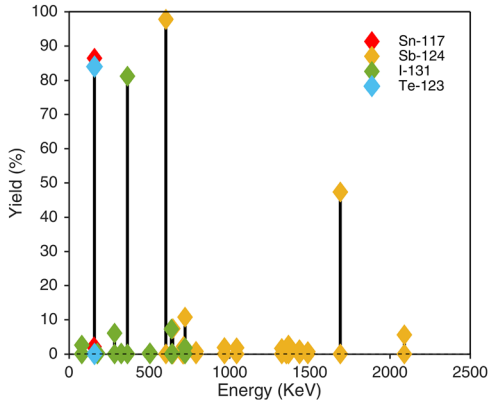

FIG. 7. Gamma-ray spectra taken on the cadmium shielded Nalgene container with the thermoelectric modules inside one week after the end of irradiation.

and antimony (Sb-124, 602.7 KeV) constituents within the TE material.

By analysing the principal nuclear reactions (Eq. 6a and 7a) which lead to the formation of new chemical species, one can estimate the mole percentage of radiation-induced doping. Initially it can be said, since Te-123 and Sn-117 are just heavier isotopes of their original species, they are not expected to lead to any significant changes in the electrical properties. Whereas, Iodine is known to be used as a doping agent for altering the electrical properties of TE materials, indicating its presence could induce performance changes.

On the other hand, Sb-124, formed by fast neutron activation of abundant Sb-123, is known to naturally decay to Te-124 as a 120-day isomer. Therefore, radiation-induced doping (I-131) and counter doping (Te-124) are simultaneously taking place within the p-type TE material while only iodine doping is taking place in the n-type material. Utilising the NGATLAS atlas of documented neutron capture cross-sections,[27] the reaction yield of iodine and antimony nuclides are calculated as,

$$Te^{130} + n \rightarrow Te^{131} + \gamma \rightarrow I^{131} + \beta^- \rightarrow Xe^{131} + \beta^- \quad (6a)$$

The absorption cross-section for Eq. 6a is ~5×10^{-27} cm^2,[27] the natural abundance of Te-130 is ~34.4% and for a fluence of 5×10^{13} neutrons cm^{-2} the number of I-131 atoms produced per initial atom of tellurium is

$$\left(5 \times 10^{-27}\right)(0.344)\left(5 \times 10^{13}\right) = 8.6 \times 10^{-14} \quad (6b)$$

Corresponding to 1.29×10^{-13} Mole % I_2 in Bi_2Te_3 and $Bi_{0.5}Sb_{1.5}Te_3$

$$Sb^{123} + n \rightarrow Sb^{124} + \gamma \rightarrow Te^{124} + \beta^- \quad (7a)$$

For Eq. 7a the absorption cross-section is ~10^{-25} cm^2,[27] the natural abundance of Sb-123 is ~43% and using the same fluence, the number of Te-124 atoms produced per initial antimony atom is

$$\left(10^{-25}\right)(0.43)\left(5 \times 10^{13}\right) = 2.15 \times 10^{-12} \quad (7b)$$

Corresponding to an additional 3.23×10^{-10} Mole % Te in $Bi_{0.5}Sb_{1.5}Te_3$

As expected, due to the bulk removal of thermal neutrons via the cadmium shielding, coupled with the use of a relatively low neutron fluence, calculated dopant mole percentages are several orders of magnitude lower than what would be required to significantly affect carrier concentration. It can therefore be assumed with confidence that the TE performance deviations to be characterized by IS is likely the result of mechanisms other than transmutation doping.

B. Impedance spectroscopy characterization

IS measurements and extracted TE properties of all pre-irradiated, post-irradiation and post-irradiation-annealed TE modules are here reported. Impedance measurements carried out in this study were repeated three times and demonstrated excellent repeatability (~1% deviation). Presented spectra are displayed as an average of each three measurements.

Figure 8 shows the experimental impedance spectra of all TE modules for pre-irradiation, post-irradiation and post-irradiation-annealed measurements. Note that module 1 was used as an experimental control and therefore was not irradiated but was measured under identical conditions. From Fig. 8, it is clearly observed that for all frequencies, post-irradiated spectra experience a notable positive shift (700 – 400 mΩ) in the real impedance Z' while the imaginary impedance Z'' shows little deviation. As expected, module 1 spectra showed little to no overall deviation, suggesting that the observed changes in modules 2 – 5 are indeed a result of neutron interactions. With regards to Eq. 1, one can interpret the shift in Z' as an overall increase in the internal ohmic resistance R_Ω of all modules. The measured increase in internal ohmic resistance can be said to directly imply an approximately equal percentage increase in the intrinsic electrical resistivity ρ of the module due to their proportional relationship, see equation Eq. 5. This increase can be said to be, in part, due to irradiation induced defects generated in the copper contacts and solder joints, as indicated by the detection of Cu-64 and Sn-117m nuclides. However, due to the vastly larger volume and thickness of TE material in comparison to the volume and thickness of the copper contacts and solder joints, neutrons with energies >1 MeV are in practice far more likely to be attenuated by the TE material. Probabilistically this indicates that a far greater number of crystallographic defects most likely lie within in the TE material itself. For modules which are designed around smaller TE couples in relation to the overall size of the device, the contribution from interconnects could be more significant.

For modules 2, 3 and 4 this increase was seen to revert after isochronal thermal annealing at 373 K, which is illustrated by the relatively equal and opposite Z' shift observed in post-irradiation-annealed spectra (Fig. 8). This is a plausible indication to the existence of a recovery mechanism which is believed to be in the form of Frenkle pair recombination. Post-irradiation-annealed spectra demonstrated no permanent change which would have been associated with transmutation doping, evidently supporting the analysis above that the concentration of transmutation reactions taking place is minimal. However, for module 5 a relatively incomplete reversal was observed before reaching the maximum service temperature (423 K) of the cold side solder. Since this module is the only one to contain polycrystalline p-type, it is believed that this occurrence is correlated with the inverse proportionality that is known to exist between the number of metallurgical boundary structures and the average mobility of Frenkle defects.[28] As the polycrystalline microstructure, will undoubtedly incorporate a greater volume of boundary structures in comparison to a monolithic structure, the annihilation of Frenkle pairs will therefore require a greater amount of kinetic energy (higher annealing temperature or longer soak time) to compensate for the subsequent reduction in mobility. A transmission electron microscope image of the metallurgical boundary structures found in a sample of polycrystalline p-type bismuth telluride is shown in Fig. 9.

For the remaining TE properties, it is known from Eq. 2 that both S and λ_{TE} are variables of R_{TE} and R_e. Hence, to graphically analyse their relative change (Fig. 4) the pure ohmic contribution R_Ω (Eq. 1) must first be eliminated by normalising Z' about a zero-mean R_Ω (Fig. 10). Initially comparing pre- and post-irradiation spectra in Fig. 10, it can be seen that no relative changes in impedance is observable below the characteristic turnover frequency ω_e, i.e. the frequency at which the vertical asymptote begins. Since this frequency is a function of the thermal diffusivity of the external isolation layer α_e (see Eq. 3), it can be said that no change to this property occurs after irradiation. This is also clearly observed in Table IV, which quantifies all the extracted parameters from the fittings. On the other hand, it is also observed that the high-mid frequency (4 kHz – 1 Hz) asymptotic rise in post-irradiation spectra

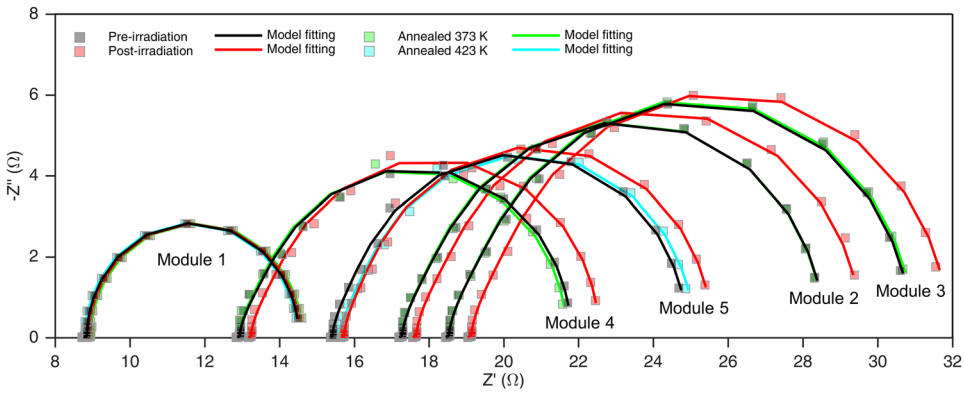

FIG. 8. Experimental impedance spectra (squares) and model fittings (solid lines) for all thermoelectric modules for pre-irradiation, post-irradiation and post-irradiation-annealed measurements.

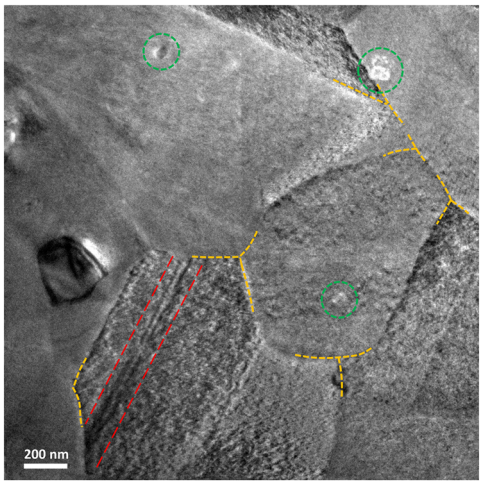

FIG. 9. Transmission electron microscope image of boundary structures within a sample of polycrystalline p-type $Bi_{0.5}Sb_{1.5}Te_3$. Markers indicate, grain boundaries (yellow lines), nanoparticles (circled in green) and crystal twinning (red lines). The image was captured using a Jeol JEM-2100.

are consistently shifted positively in the real axis Z', i.e. an increase in R_e (Fig. 4). With regards to Eq. 5, this increase can be said to either be due to an increase in the Seebeck coefficient S of the thermoelements or a reduction of the thermal conductivity of the external alumina layer λ_e. Since the work by Snead *et al.*[29] experimentally demonstrated that meaningful reduction of the thermal conductivity of common ceramics plates (such as alumina) generally occurs for fluencies $>1 \times 10^{20}$ neutrons cm^{-2}, it can be deduced that an increase in S is more probable.

Turning attention to the mid-low frequency (1 Hz – 1 mHz) region of Fig. 10 spectra, it can be observed that a consistent broadening in the real plane (800 – 600 mΩ) of the dominant Warburg-type semicircle for all TE modules occur after irradiation. Once again, looking at Fig. 4, it can be interpreted that this broadening effect corresponds to an increase in R_{TE} and R_e due to convective contributions coupling both resistances. Note that if in-vacuum measurements were undertaken then changes to R_{TE} could be isolated.

Nevertheless, irradiation induced broadening of the Warburg-type semicircle and positive asymptotic shifting can be seen to consistently revert towards its pre-irradiation state after sufficient thermal annealing. Once again, this hints at the existence of a recovery mechanism, most likely in the form of Frenkle pair recombination as previously discussed.

To more specifically quantify the relative changes in R_Ω, R_{TE} and R_e due to irradiation, the previously outlined model (Eq. 1) was fitted to pre-irradiation, post-irradiation and post-irradiation-annealed spectra illustrated in Fig. 8 and Fig. 10, and corresponding TE properties were extracted. All pre-irradiated TE properties and their change due to irradiation are summarised in Table IV. The model fittings can be seen to indicate an average relative increase in absolute Seebeck coefficient S (~3%), internal

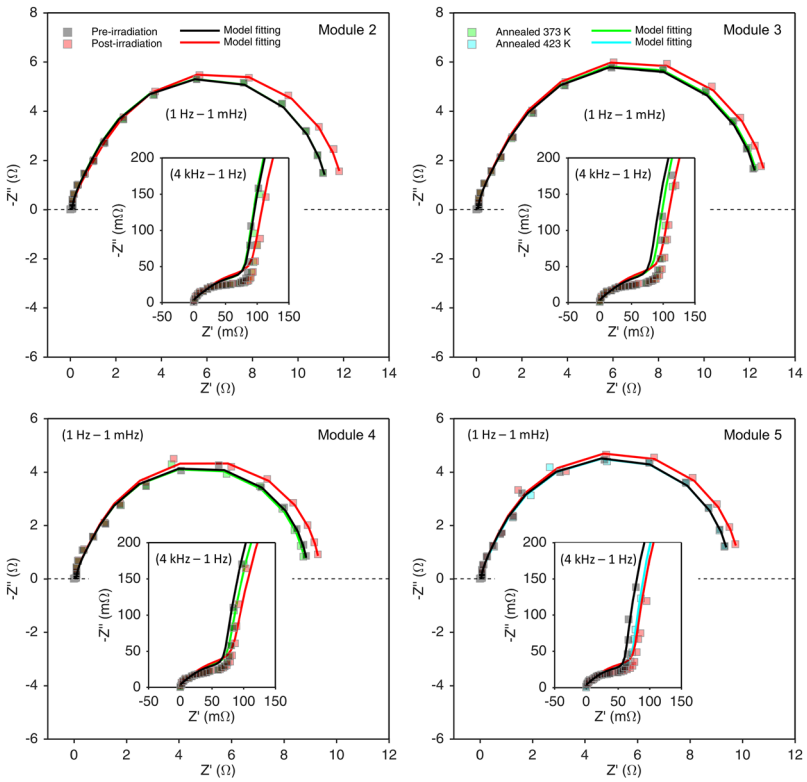

FIG. 10. Normalised Nyquist plot of each thermoelectric module pre-irradiation, post-irradiation and post-irradiation annealed. The inset details a magnification of the high-mid frequency area.

TABLE IV. Summary of fitted parameters and maximum associated fitting errors (calculated using Monte-Carlo residual resampling[12]) obtained for all measured impedance spectra.

		zT ±0.001	S (μVK^{-1}) ±1	λ_{TE} (Wm^{-1}K^{-1}) ±0.02	ρ (μΩm) ±0.01	R_Ω (Ω) ±0.01	R_{TE} (Ω) ±0.01	R_e (mΩ) ±2	ω_{TE} (mHz) ±0.3	ω_e (Hz) ±0.1
Module 1 (Control)	Pre-rad	0.68	230	2.32	4.90	8.76	5.96	185	6.37	2.23
	Post-rad	0.68	229	2.29	4.91	8.78	5.99	183	6.45	2.26
	Annealed	0.68	230	2.31	4.92	8.80	5.99	185	6.32	2.24
Module 2	Pre-rad	0.68	248	2.80	9.61	17.20	11.67	214	4.49	2.42
	Post-rad	0.71	255	2.78	9.82	17.57	12.49	228	4.44	2.43
	Annealed	0.68	248	2.81	9.60	17.18	11.68	214	4.56	2.42
Module 3	Pre-rad	0.68	250	2.68	10.28	18.39	12.48	218	4.39	2.21
	Post-rad	0.70	256	2.67	10.65	19.05	13.27	229	4.38	2.23
	Annealed	0.68	251	2.68	10.32	18.47	12.52	219	4.41	2.23
Module 4	Pre-rad	0.73	233	2.32	9.59	12.87	9.38	190	5.41	2.71
	Post-rad	0.76	239	2.30	9.80	13.15	9.97	200	5.73	2.75
	Annealed	0.73	231	2.34	9.57	12.84	9.36	191	5.65	2.69
Module 5	Pre-rad	0.63	198	1.62	11.45	15.36	9.75	138	5.21	2.58
	Post-rad	0.66	204	1.61	11.74	15.75	10.38	146	5.27	2.59
	Annealed	0.63	200	1.64	11.58	15.53	9.76	139	5.30	2.63

resistance R_Ω (~3%) and intrinsic resistivity ρ (~3%) for post-irradiation spectra. Hence, despite the applied neutron fluence inducing an increase to the ohmic resistivity of the module, an average enhancement of the TE power factor S^2/ρ of ~3% was found. Intriguingly, since a non-significant decrease was observed for the thermal conductivity λ_{TE} (<2%) of the Thermoelements, an overall improvement to zT of ~4% was documented on average for all modules.

However, irrespective of this, modules 2, 3 and 4 demonstrated the capability to fully anneal away induced changes at 373 K which is expected to be around the average operating temperature across a TE module during service. This indicated that a minimum of 50% of the module's thermocouple volume will most likely be continuously annealed during service. Module 5 on the other hand was shown to require an annealing temperature greater than 423 K, implying that greater than 75% of the module's thermocouple volume will not undergo continuous annealing (assuming a 473 K hot side and 273 K cold side) during in-service operation. It should therefore be noted that Bi_2Te_3 based alloys which are manufactured with a polycrystalline microstructure could have greater susceptibility to induced performance changes from neutron irradiation. Though, a more representative analysis of thermal annealing characteristics would be one in which TE modules are irradiated while operating under an application specific thermal gradient. This aspect could be focused upon in a potential follow-up study.

IV. CONCLUSIONS

In this study, four Bi_2Te_3 based thermoelectric modules were irradiated by fast neutrons with a total fluence equivalent to the neutron yield expected from a 50 W_e Americium-241 radioisotope thermoelectric generator with a 10-year nominal mission. Gamma-ray spectrographic analysis of the post-irradiated modules indicated the initial formation of many short-lived nuclides, Na-24, Mn-54, Cu-64, Sb-122 and La-140 followed by longer lasting nuclides which are believed to originate from the mutation of lead solder joints (Sn-117m) as well as from the thermoelectric materials (Te-123m, I-131 and Sb-124). The principal nuclear reactions showed radiation-induced dopants concentrations are several orders of magnitude lower than what is required to cause a change to thermoelectric properties based on previous literature. Moreover, no permanent change in impedance spectra was observed for post-irradiated-annealed modules, supporting this conclusion. Impedance spectroscopy measurements of post-irradiated modules revealed a systematic shift and broadening of impedance spectra. This translated to an overall relative increase in absolute Seebeck coefficient (~3%), internal resistance (~3%) and intrinsic resistivity (~3%), i.e. a ~3% absolute increase in thermoelectric power factor. Since thermal conductivity showed no meaningful change (<2%), zT was found to increase on average by ~4%. Intriguingly, post-irradiation annealing of all modules revealed polycrystalline based modules have greater susceptibility to irradiation effects. Nevertheless, as the perceived changes are relatively small and more importantly positive, all modules presented in this study can be said to display more than sufficient radiation hardness for an Americium-241 radioisotope thermoelectric generator application. Notably, this study showcases an exciting potential for characterising and monitoring in-service degradation of practical thermoelectric modules using impedance spectroscopy.

ACKNOWLEDGMENTS

Funding for RM was provided in part via EPSRC grants EP/L505006/1, EP/M506564/1 and EP/M508081/1. JGC acknowledge financial support from the Spanish Agencia Estatal de Investigación under the Ramón y Cajal program (RYC-2013-13970) and from the Universitat Jaume I under the project UJI-A2016-08. The authors gratefully acknowledge the assistance provided by, the Ohio State University Research Reactor team, the European Space Agency and the role of the EPSRC TE Network in fostering the collaboration.

SUPPLEMENTARY MATERIAL

See supplementary material for the gamma and impedance spectroscopy data required to reproduce these findings.

NOMENCLATURE

Symbol

Z	Impedance (Ω)
R	Resistance (Ω)
ρ	Resistivity (Ωm)
ω	Angular frequency (rad s^{-1})
S	Seebeck Coefficient (VK^{-1})
α	Thermal diffusivity (m^2s^{-1})
λ	Thermal conductivity ($Wm^{-1}K^{-1}$)
h	Convective transfer coefficient ($Wm^{-2}K^{-1}$)
T	Temperature (K)
A	Area (mm^2)
L	Length or thickness (mm)
η	Filling factor
N	Number of thermoelectric couples
j	Imaginary number
J_i	Bessel function of i order
δ_n	n^{th} zero root of J_1

Subscript

i	Initial
TE	Thermoelectric leg
e	External alumina layer
o	Module outer surface
h	Convective surface
SC	Spreading-Constriction
Weo	Open Warburg impedance
Ω	Internal ohmic resistance

REFERENCES

[1]D. P. Kramer, R. Ambrosi, M. Sarsfield, E. J. Watkinson, R. Mesalam, H. Williams, C. Barklay, T. Tinsley, S. Goodrich, T. Pierson, and C. Whiting, "Recent joint studies related to the development of space radioisotope power systems," E3S Web Conf **16**, 5002 (2017).

[2]L. Summerer and K. Stephenson, "Nuclear power sources: A key enabling technology for planetary exploration," Proc Inst Mech Eng Part G J Aerosp Eng **225**, 129–143 (2011).

[3]G. L. Bennett, "Mission interplanetary: Using radioisotope power to explore the solar system," Energy Convers Manag **49**, 382–392 (2008).

[4]E. J. Watkinson, R. M. Ambrosi, H. R. Williams, M. J. Sarsfield, K. Stephenson, D. P. Weston, N. Marsh, and C. Haidon, "Cerium neodymium oxide solid solution synthesis as a potential analogue for substoichiometric AmO 2 for radioisotope power systems," J Nucl Mater **486**, 308–322 (2017).

[5]E. J. Watkinson, R. M. Ambrosi, D. P. Kramer, H. R. Williams, M. J. Reece, K. Chen *et al.*, "Sintering trials of analogues of americium oxides for radioisotope power systems," J Nucl Mater **491**, 18–30 (2017).

[6]H. R. Williams, R. M. Ambrosi, K. Chen, U. Friedman, H. Ning, M. J. Reece, M. C. Robbins, K. Simpson, and K. Stephenson, "Spark plasma sintered bismuth telluride-based thermoelectric materials incorporating dispersed boron carbide," J Alloys Compd **626**, 368–374 (2015).

[7]R. C. O'Brien, R. M. Ambrosi, N. P. Bannister, S. D. Howe, and H. V. Atkinson, "Safe radioisotope thermoelectric generators and heat sources for space applications," J Nucl Mater **377**, 506–521 (2008).

[8]C. Lin, Z. Zhang, U. K. Mishra, S. Barbara, and L. Brillson, "Neutron irradiation effects on metal-gallium nitride contacts neutron irradiation effects on metal-gallium nitride contacts," J Appl Phys 123705 (2015).

[9]J. García-Cañadas and G. Min, Chapter 6, *High-throughput Thermoelectric Measurement Techniques*, n.d., p. 133–155.

[10]C.-Y. Yoo, Y. Kim, J. Hwang, H. Yoon, B. J. Cho, G. Min, and S. H. Park, "Impedance spectroscopy for assessment of thermoelectric module properties under a practical operating temperature," Energy (2017).

[11]J. García-Cañadas and G. Min, "Impedance spectroscopy models for the complete characterization of thermoelectric materials," J Appl Phys **116**, 174510 (2014).

[12]R. Mesalam, H. R. Williams, R. M. Ambrosi, J. García-Cañadas, and K. Stephenson, "Towards a comprehensive model for characterising and assessing thermoelectric modules by impedance spectroscopy," Appl Energy **226**, 1208–1218 (2018).

[13]D. K. Aswal, R. Basu, and A. Singh, "Key issues in development of thermoelectric power generators: High figure-of-merit materials and their highly conducting interfaces with metallic interconnects," Energy Convers Manag **114**, 50–67 (2016).

[14]H. H. Saber, M. S. El-Genk, and T. Caillat, "Tests results of skutterudite based thermoelectric unicouples," Energy Convers Manag **48**, 555–567 (2007).

[15]H. Wang and K. J. Leonard, "Effect of high fluence neutron irradiation on transport properties of thermoelectrics," Appl Phys Lett **111**, 43901 (2017).

[16]M. Idnurm and K. Landecker, "Changes produced in thermoelectric materials by thermal-neutron irradiation," Br J Appl Phys **18**, 1209–1211 (1967).

[17]J. C. Corelli and R. T. Frost, *The Effects of Reactor Irradiation on The Thermoelectric Properties of Lead and Bismuth Tellurides* (1960).

[18]W. J. Parker, R. J. Jenkins, C. P. Butler, and G. L. Abbott, "Flash method of determining thermal diffusivity, heat capacity, and thermal conductivity," J Appl Phys **32**, 1679–1684 (1961).

[19]R. D. Cowan, "Pulse method of measuring thermal diffusivity at high temperatures," J Appl Phys **34**, 926–927 (1963).

[20]L. M. Clark III and R. E. Taylor, "Radiation loss in the flash method for thermal diffusivity," J Appl Phys **46**, 714–719 (1975).

[21]H. Wang, W. D. Porter, H. Böttner, J. König, L. Chen, S. Bai *et al.*, "Transport properties of bulk thermoelectrics—An international Round-Robin study, Part I: Seebeck coefficient and electrical resistivity," J Electron Mater **42**, 654–664 (2013).

[22]H. Wang, W. D. Porter, H. Böttner, J. König, L. Chen, S. Bai *et al.*, "Transport properties of bulk thermoelectrics: An international Round-Robin study, Part II: Thermal diffusivity, specific heat, and thermal conductivity," J Electron Mater **42**, 1073–1084 (2013).

[23]E. P. Wigner, "Theoretical physics in the metallurgical laboratory of Chicago," J Appl Phys **17**, 857–863 (1946).

[24]C. Claeys and E. Simoen, "Basic Radiation Damage Mechanisms in Semiconductor Materials and Devices," *Radiat. Eff. Adv. Semicond. Mater. Devices*, vol. 57, Berlin, Heidelberg, Springer Berlin Heidelberg, 2002, p. 9–52.

[25]A. F. Ioffe, *Physics of Semiconductors* (Acad New York, 1960).

[26]M. Izerrouken, Y. Djouadi, and H. Zirour, "Nuclear instruments and methods in physics research B annealing process of F^- and F^+-centers in Al_2O_3 single crystal induced by fast neutrons irradiation," Nucl Inst Methods Phys Res B **319**, 29–33 (2014).
[27]J. Kopecky, Ch. Sublet J, J. A. Simpson, R. A. Forrest, and D. Nierop, *IAEA: Atlas of neutron capture cross sections* (Vienna, Austria, 2010).
[28]B. P. Uberuaga, L. J. Vernon, E. Martinez, and A. F. Voter, "The relationship between grain boundary structure, defect mobility and grain boundary sink efficiency," Sci Rep **5**, 9095 (2015).
[29]L. L. Snead, S. J. Zinkle, and D. P. White, "Thermal conductivity degradation of ceramic materials due to low temperature, low dose neutron irradiation," J Nucl Mater **340**, 187–202 (2005).